

Background Study on ν_e Appearance from a ν_μ Beam in Very Long Baseline Neutrino Oscillation Experiments with a Large Water Cherenkov Detector

C. Yanagisawa*, C. K. Jung, P. T. Le†

Department of Physics and Astronomy, Stony Brook University, Stony Brook, NY 11794-3800, U.S.A.

B. Viren

Department of Physics, Brookhaven National Laboratory, Upton, NY 11973, U.S.A.

(Dated: November 20, 2021)

There is a growing interest in very long baseline neutrino oscillation experimentation using accelerator produced neutrino beam as a machinery to probe the last three unmeasured neutrino oscillation parameters: the mixing angle θ_{13} , the possible CP violating phase δ_{CP} and the mass hierarchy, namely, the sign of Δm_{32}^2 . Water Cherenkov detectors such as IMB, Kamiokande and Super-Kamiokande have shown to be very successful at detecting neutrino interactions. Scaling up this technology may continue to provide the required performance for the next generation of experiments. This report presents the latest effort to demonstrate that a next generation (> 100 kton) water Cherenkov detector can be used effectively for the rather difficult task of detecting ν_e s from the neutrino oscillation $\nu_\mu \rightarrow \nu_e$ despite the large expected potential background resulting from π^0 s produced via neutral current interactions.

PACS numbers: 13.15.+g, 14.60.Lm, 14.60.Pq

Keywords: neutrino oscillation, water Cherenkov

I. INTRODUCTION

It has been shown that there are certain advantages in a wideband neutrino beam over a now traditional narrow-band neutrino beam for neutrino oscillation experiments, especially for the observation of $\nu_\mu \rightarrow \nu_e$ oscillation, provided that the baseline is reasonably long (over 1,000 km) [1].

By broadening the range of energies with which multiple oscillations can be resolved, a richer parameter space can become accessible than is available to an experiment focused on only the first oscillation maximum.

In the original paper proposing the use of a wide-band neutrino beam for a very long baseline neutrino oscillation (VLBNO) experiment [1] by the Brookhaven National Laboratory (BNL) neutrino working group (NWG) some simplifying assumptions were used. The sensitivities presented in the paper relied on calculations based on 4-vector level Monte Carlo (MC) simulations, a simple model for energy resolution and certain assumptions about reconstruction capabilities. Namely, a detailed detector simulation for the proposed water Cherenkov detector was not included. In addition it was assumed that the signal events were only from quasi-elastic (QE) charged current (CC) scattering ($\nu_e + n \rightarrow e^- + p$) and the background events were only from single π^0 neutral

current (NC) interactions $\nu + N \rightarrow \nu + \pi^0 + N'$ where N and N' are nucleons.

In order to gain a better insight on this idea of the VLBNO experiment with a wide-band neutrino beam for $\nu_\mu \rightarrow \nu_e$ oscillation, we performed a more sophisticated and elaborate multivariate likelihood based analysis using a full MC simulation that included inelastic neutrino interactions, water Cherenkov detector response, and well-tuned event reconstruction algorithms. This MC simulation and reconstruction programs were developed and fine-tuned for the Super-Kamiokande-I experiment (SK-I) [2].

II. ENERGY RECONSTRUCTION AND EVENT DESCRIPTION

For the discussions in this paper, we calculate a reconstructed neutrino energy using the formula

$$E_{rec} = \frac{m_N E_e}{m_N - (1 - \cos\theta_e) E_e},$$

where m_N , E_e and θ_e are the nucleon mass, the recoil electron energy and the scattering angle of the recoil electron with respect to the incident neutrino beam, respectively. In a strict sense, this quantity represents the incident neutrino energy only when the event is produced by CC QE scattering and the Fermi motion of target nucleons is ignored. Nonetheless, we show in Figure 1 the neutrino energy and E_{rec} for CC QE (top) and all CC (bottom) events to compare the two energy distributions for the two classes of CC events. Although E_{rec} for the CC events does not reproduce the incident neutrino

*email: chiaki@nngroup.physics.sunysb.edu; Also at Science Department, BMCC, City University of New York, 199 Chambers Street, New York, NY 10007, U.S.A.

†Currently, Department of Physics and Astronomy, Rutgers, the State University of New Jersey, 136 Frelinghuysen Rd, Piscataway, NJ 08854

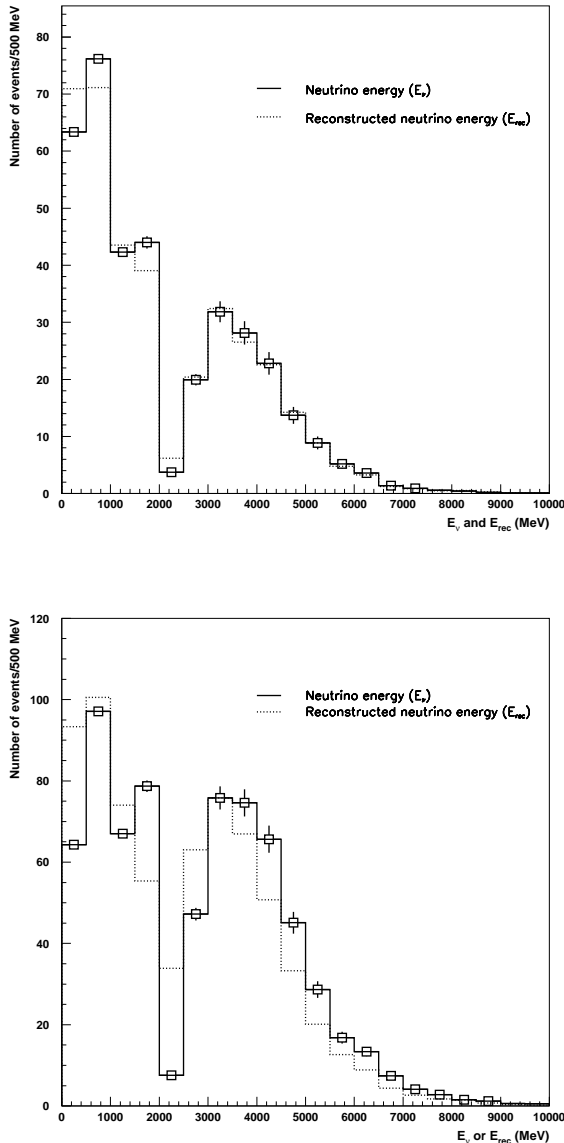


FIG. 1: The distributions of neutrino energy (E_ν) and reconstructed neutrino energy ($E_{\nu_{rec}}$) of single ring e-like events originating from CC QE interactions (top figure) and from all CC interactions (bottom figure). Note that a dip at about 2 GeV is due to $\nu_\mu \rightarrow \nu_e$ neutrino oscillation. The open square boxes with error bars indicate statistical uncertainties.

spectrum as well as it does for CC QE events, it still reproduces it quite well.

The initial event selection is made to maximize the number of interactions that are consistent with coming from ν_e appearing at the far end of the baseline in the beam while minimizing events such as ν_μ CC or any events from NC interactions. Needless to say, the clearest event signature comes from ν_e CC QE interactions. Inelastic ν_e CC events also carry information about os-

cillations but are more difficult to cleanly select and have somewhat worse energy resolution as shown in Figure 1. Regardless of the interaction, a recoil proton will rarely be above its Cherenkov threshold of about 1.25 GeV/c and will not contribute notably to the event signature. For these reasons, a ν_e appearance candidate event will be initially selected if its signature is consistent with being a Cherenkov radiation pattern from a single electron (termed *single ring, e-like*).

A ν_μ CC QE event will usually be distinguishable from one arising from a ν_e CC QE interaction as the resulting Cherenkov ring produced by ν_μ will have a sharper rise and fall in the amount of Cherenkov light at the edges of the ring than one due to an electron. This is because a muon presents a relatively straight line source of Cherenkov light while an electron initiates an electromagnetic shower. This shower consists of a distribution of track directions due to the number of particles in the shower and that they experience larger multiple scattering. As the muon energy approaches the Cherenkov threshold there is an increasing chance that multiple scattering and the collapsing Cherenkov light cone will smooth the rise of the edge of the ring and potentially mimic an electron.

Likewise, inelastic and NC interactions with a non-zero pion multiplicity can have additional light that is not consistent with the pattern of a single e-like ring. Depending on the exact event topology these events are either easily ruled out or present challenging backgrounds. Charged pions above their Cherenkov threshold of 160 MeV/c produce a μ -like ring and are rejected. Events with visible light from both pions and the primary charged lepton are strongly rejected based on ring counting.

Events with a final state consisting of only a single neutral pion present a particular challenge. The π^0 decays to a pair of gamma rays, each of which initiate an electromagnetic shower and produce an e-like ring of varying intensity and direction. These π^0 events can become background depending on how the π^0 decays to two gamma rays. At one extreme, the decay is symmetric such that the gamma rays have similar energies. If the original π^0 is boosted enough, the two gamma rays are nearly collinear and produce mostly overlapping rings. They can then be impossible to be distinguished single electron events with an energy equal to the sum of the two gammas. At the other extreme, a highly asymmetric π^0 decay results in one strongly boosted and one strongly retarded gamma ray. In the lab frame, the higher energy gamma will produce a single e-like ring while the other may produce no discernible light.

The events with a π^0 in the final state can come from two sources: (1) NC interactions and (2) charge exchanges of charged pions inside the target nucleus or with an oxygen or a hydrogen nucleus while traveling in water.

Finally, there are events from electron neutrino interactions that are not from ν_e that appeared in the beam from neutrino oscillation $\nu_\mu \rightarrow \nu_e$. Rather, there is an intrinsic ν_e component in the unoscillated neutrino beam

originating from muon or kaon decays. The beam used in this study has an intrinsic ν_e component which is 0.7% of the ν_μ flux. The background events from these neutrinos are irreducible.

In this analysis, to classify the events for the initial selection, the reconstruction algorithms used for the SK-I atmospheric neutrino analysis are employed. In addition, a special algorithm called *POLfit* [8] is used. This algorithm has been found to be extremely useful for removing single π^0 background events in samples containing events that are classified as single-ring and e-like [9] by the standard SK-1 reconstruction. This paper describes how information provided by *POLfit*, together with other useful variables, can be effectively used to significantly reduce the π^0 background while retaining a sufficient efficiency for the signal.

III. MONTE CARLO EVENT SAMPLE

The Monte Carlo event sample used in this study was originally produced by the SK-I collaboration to simulate atmospheric neutrino events detected by the SK-I detector and corresponds to about 100 years of the exposure. The detailed description of the Monte Carlo generation as well as the event reconstruction is described elsewhere [3].

The energy spectra for ν_μ and ν_e produced in the Earth's atmosphere are different from those in the neutrino beam proposed by the BNL NWG. To account for this, each ν_μ event is given a weight based on the neutrino energy such that the shape of the resulting spectrum matches that expected from the beam. An additional normalization is applied so that the total number of ν_μ CC QE events is as expected.

Assuming no oscillations, it is expected that there will be 12,000 such events for a detector with SK-I efficiencies and fiducial volume of 500 kton ($22.2 \times$ SK-I) which is placed 2,540 km from the neutrino production target and for five years of running as described in the paper by BNL NWG [1]. When oscillations are applied, this sample is weighted by the oscillation probability taking into account full three-neutrino mixing and matter effects.

The oscillated ν_e sample is prepared by similarly weighting and normalizing the ν_e atmospheric MC events to what is expected from the ν_μ component of the beam, that is, under the assumption of 100% $\nu_\mu \rightarrow \nu_e$ oscillation. Actual oscillation parameters are then applied to this sample by weighting to the appropriate oscillation probability. The intrinsic ν_e component in the beam is taken to be the shape predicted by the beam MC simulation and is normalized to be 0.7% that of the ν_μ component. To include the effect of neutrino oscillation, the contribution of the ν_e component is calculated only when ν_e survives as ν_e at the water Cherenkov detector placed at a given baseline.

The expected numbers of the events to be observed from the intrinsic anti- ν_μ component of the beam are estimated to be 2.2% and 2.5% of the expected numbers

of the background events from the ν_μ (background-1) for the baselines of 2,540 km and of 1,480 km, respectively (see the next section for the description about the baseline). The expected numbers of the events to be observed from anti- ν_e component of the beam are estimated to be less than 4.5% and 4.3% of the expected numbers of the background events from the intrinsic ν_e component of the beam (background-2) for the baselines of 2,540 km and of 1,480 km, respectively. Since these contributions are much smaller than the events from the background-1 and the background-2, although not negligible, we will not take into account them further in this report.

To select MC ν_e appearance candidate events an initial set of cuts based on the standard SK-I codes is used: (a) there is one and only one e-like ring, (b) the reconstructed event vertex is at least 2 m from any inner photomultiplier (PMT) surface and (c) there is no activity in the outer (veto) detector.

In addition to these standard cuts, events produced by neutrinos with energies greater than 10 GeV are ignored due to lack of statistics in the atmospheric MC sample. The beam has a tail that extends up to 15 GeV but its contribution to the background is negligible as will be shown below.

IV. NEUTRINO OSCILLATION PROBABILITIES

The oscillation probabilities applied to the components of the beam neutrino flux use the following parameters:

$$\begin{aligned} \Delta m_{21}^2 &= 7.3 \times 10^{-5} eV^2, \\ \Delta m_{31}^2 &= 2.5 \times 10^{-3} eV^2, \\ \sin^2 2\theta_{12} &= 0.86, \\ \sin^2 2\theta_{23} &= 1.0, \\ \sin^2 2\theta_{13} &= 0.04, \text{ and} \\ \delta_{CP} &= 0^\circ, \pm 45^\circ, \pm 135^\circ. \end{aligned}$$

Note that the sign convention of δ_{CP} follows that of the paper by BNL NWG [1]. Unless otherwise stated, in this paper the value of δ_{CP} is $+45^\circ$ and the baseline is 2,540 km which corresponds to the distance from BNL to Homestake Mine in South Dakota. Later we will describe the results with different values for δ_{CP} as well as with the baseline of 1,480 km which corresponds to the distance from Fermilab to Henderson Mine in Colorado. The result with the baseline of 1,480 km was for the UNO detector proposed first in 1999 and later to be built in Henderson Mine. See the references [4] for the detail of the UNO detector. These results are similar to what is expected for the Fermilab to Homestake baseline of 1,300km. This shorter baseline is considered by applying inverse-square scaling of the flux and recalculation of oscillation probabilities.

The neutrino oscillation probabilities were calculated by the *nuosc* [5] package. The calculator assumes 3- ν oscillation with possible CP symmetry violation and matter effects. The matter densities can be vacuum, non-zero

constant or stepwise-constant matter densities. The non-constant PREM [6] and arbitrary user provided density profiles are also supported. It calculates the probabilities either analytically for constant matter densities or for any density profile it can use a 5th order adaptive Runge-Kutta stepper. The package has been validated against published calculations [7].

V. POLFIT

In this section we briefly describe the π^0 fitter called *Pattern Of Light fit (POLfit)* [8]. *POLfit* is applied to events which are initially classified as single-ring and e-like by the standard SK-I analysis codes in order to identify π^0 background events in this event sample. It assumes the event is a π^0 event and that the ring found by the standard codes is one of the gammas from the π^0 decay. It will then determine the direction and energy of a secondary gamma that, along with the primary one, is most consistent with the pattern of light collected by the PMTs. *POLfit* produces two possible secondary gammas by employing two algorithms. One is optimized assuming the secondary ring is overlapping with the primary ring (forward-algorithm). The other is optimized to find a second ring in the wider angular region (wide-algorithm).

In each algorithm, the pattern of light expected from the full π^0 decay is calculated from a set of templates and compared to the collected light and a likelihood is formed. These templates are pre-determined using the detector simulation. The energy and direction phase-space of the secondary gamma is searched to find the point that leads to the maximum likelihood. Each algorithm supplies the direction of two photons, their energies, the two photon invariant mass, and the maximum likelihood value obtained. It was found that the wide-algorithm method more reliably finds a real second ring more often than the forward-algorithm. Therefore, in this report we use mostly the information provided by the wide-algorithm unless otherwise stated.

To demonstrate the power of *POLfit*, Figure 2 shows the relative π^0 reconstruction efficiencies with (solid circles) and without (open circles) *POLfit* employed as a function of the opening angle between the two reconstructed gammas from the π^0 decay in the lab frame and for single π^0 events produced by the NC interactions. To be accepted in this sample, the event must have a two-photon invariant mass ($m_{\gamma\gamma}$) within 2σ of the expected value given the event came from a π^0 . Here, the neutrino energy spectrum is that of the original SK-I atmospheric muon neutrinos. In the case without *POLfit*, only events identified as having two e-like rings by the standard SK-I software can be candidates to be a π^0 . With *POLfit* information, π^0 events that are classified as single-ring by the standard selection may now be selected.

Depletion of π^0 detection efficiencies at a small opening angle is due to overlap of the two e-like rings. At

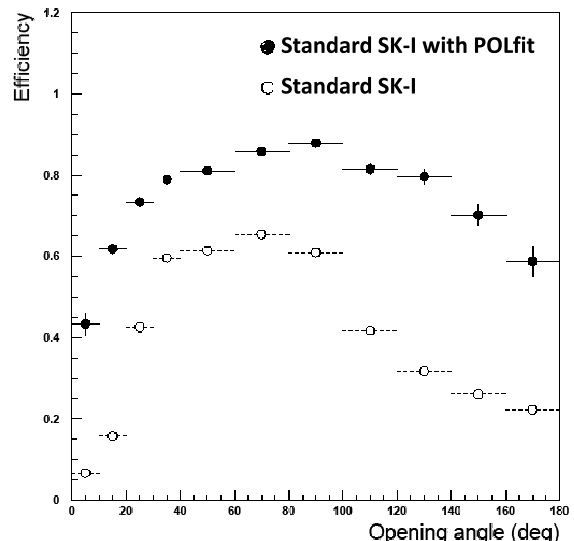


FIG. 2: π^0 reconstruction efficiency with the standard SK-I codes (open circles) and after accepting additional events with missing gamma found by *POLfit* (solid circles).

large opening angle it is due to the second ring being too faint. As clearly seen in Figure 2, *POLfit* improves the π^0 reconstruction efficiency significantly.

VI. USEFUL VARIABLES TO DISTINGUISH THE SIGNAL FROM THE BACKGROUND

A cut on $m_{\gamma\gamma}$ reduces background from single π^0 NC events but it also reduces signal efficiency somewhat. Alone, it is not enough to reduce the background to a level comparable to the oscillation signal. It is, therefore, desirable to find additional distinguishing features.

In this section, nine such features (variables) including $m_{\gamma\gamma}$ are described. Distributions of these variables are shown for events that are oscillated ν_e CC (labeled “signal” and with solid lines) and NC, ν_μ CC and beam- ν_e CC events (“background”, dotted lines). The distributions are plotted for different E_{rec} regions in steps of 0.5 GeV from 0 to 2 GeV, $2 \text{ GeV} \leq E_{rec} < 3 \text{ GeV}$ and $E_{rec} \geq 3 \text{ GeV}$.

In general, at lower energies (sub-GeV range), the background is largely from the misidentified single- π^0 events discussed above. At higher energies, non-QE interactions become dominant leading to additional ways for background to mimic ν_e CC QE events.

A. Reconstructed π^0 mass ($m_{\gamma\gamma}$)

As shown above, this variable is useful to remove background events that come from single π^0 NC production. In Figure 3 the distributions of $m_{\gamma\gamma}$ are shown. In the lower reconstructed neutrino energy region ($E_{rec} \leq 2$

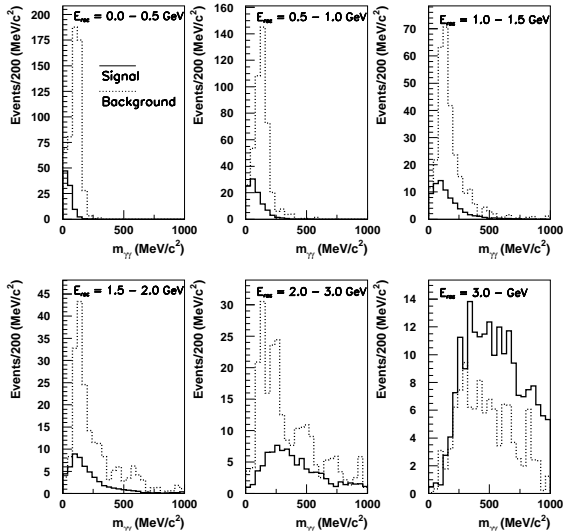


FIG. 3: The distributions of reconstructed π^0 mass of single e-like ring events for signal (solid line) and background (dotted line).

GeV), the distributions show a prominent π^0 peak. At higher energies, the contribution from multi-pion production increases and *POLfit* begins to reconstruct the correct second gamma poorly or returns an arbitrary result that is not associated with any physical particle. Because of this, the π^0 peak disappears in the higher energy region.

B. Fraction of energy in the second ring (E_{frac})

In general, the second e-like ring found by *POLfit* has less energy than the one found by the standard SK-I reconstruction software. Furthermore, *POLfit* must find a second ring and if the event does not in fact have one, this wrongly reconstructed ring tends to have much less energy than the primary one. This effect is shown in Figure 4 where the ratios of the energy of the second ring to the sum of two ring energies are plotted.

C. Difference in $\log \pi^0$ likelihood ratio ($\Delta \log \pi^0\text{-lh}$)

As mentioned above, *POLfit* employs two algorithms, the wide- and forward-algorithm. Each provides a log-likelihood that the event is a π^0 . Signal events actually contain only a single ring. Nevertheless, with such events, *POLfit* will return a second, fake ring. In such cases, both algorithms tend to place this fake ring in the vicinity of the single primary ring. Therefore, the two algorithms tend to find similar fake rings. This makes the two likelihoods similar to each other and the log-likelihood ratio

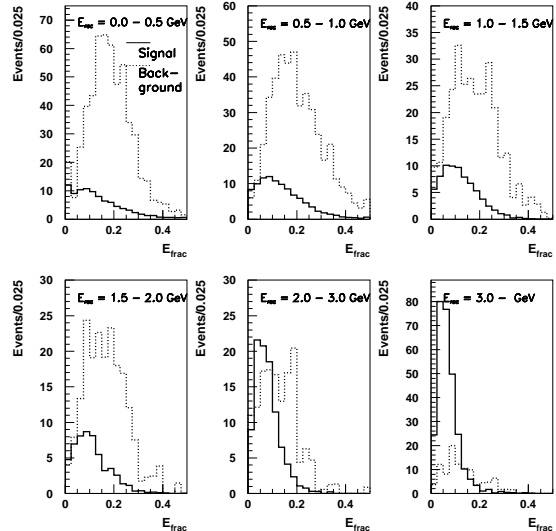


FIG. 4: The distributions of the energy fraction of the second ring found by *POLfit* in 1-ring events for the signal (solid line) and background (dotted line).

(difference between two log-likelihoods) tends to be symmetric around zero. On the other hand, in the case of a π^0 background event the secondary photon from a π^0 decay is not necessarily confined in the direction of the primary photon. This makes the log-likelihood ratio asymmetric with a long left tail, especially at lower energies. The difference is significant in the lower energy region as shown in Figure 5. However, this trend changes above $E_{rec} = 1.0$ GeV where the contribution from multi-pion production starts to increase and dilutes this effect.

D. Direction cosine of the e-like ring ($\cos\theta$)

The direction cosine of the primary e-like ring with respect to the neutrino beam is a good discriminator to separate the signal from the background. Its distributions are shown in Figure 6. This variable does not depend on the information from *POLfit*.

As the energy of the neutrino decreases, the outgoing electron direction is distributed over a wider angle with respect to the neutrino direction. As the energy becomes comparable to that of Fermi motion, the distribution is further widened because the momentum of the target nucleon becomes significant and will tend to randomize the electrons direction. This latter effect is less for the more massive π^0 .

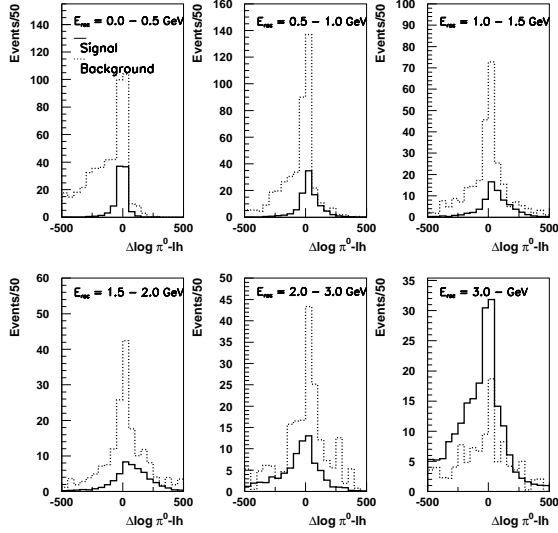


FIG. 5: The distributions of the difference in $\log \pi^0$ likelihood between the two algorithms. The larger this variable, the more likely an event is the π^0 background. The distributions in solid lines are for the signal and those in dotted lines are for the background.

E. Total charge to ring energy ratio (Q/E)

Light collected in an event that is not consistent with the single ring found by the standard SK-I codes is an indication of unreconstructed or missed particles and thus a non-QE interaction. A measure of this light is the ratio of the total charge, in unit of PE (photoelectron), collected by all PMTs to the energy associated with the primary reconstructed ring in MeV. Some background events where only one ring is found are expected to produce some light which is not identified as a ring. The distributions of this variable are shown in Figure 7. The separation is most pronounced at lower reconstructed energy where any π^0 s are likely to be less boosted and not put all their light in the forward direction. Thus in an asymmetric π^0 decay the second ring tends to be weaker than the standard SK codes can detect.

F. \log particle-identity-likelihood ($\log \text{pid-lh}$)

The standard SK-I reconstruction software provides likelihoods of a Cherenkov ring to be e-like (L_e) and μ -like (L_μ). From these two likelihoods, the logarithm of the ratio of likelihoods, $\log(L_\mu/L_e)$ ($\log \text{pid-lh}$) is used as a good measure to separate electrons from muons. The more negative $\log \text{pid-lh}$ is, the more e-like a Cherenkov ring is. When two e-like rings, such as the photons from a π^0 decay, overlap and reconstruct as a single ring they can produce a $\log \text{pid-lh}$ that is more e-like than a single

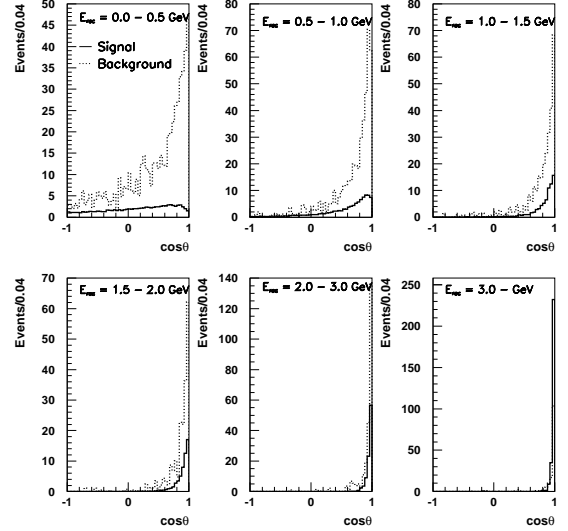


FIG. 6: The distributions of the directional cosine of the primary e-like ring with respect to the neutrino beam direction. The distributions in solid lines are for the signal and that in dotted lines are for the background.

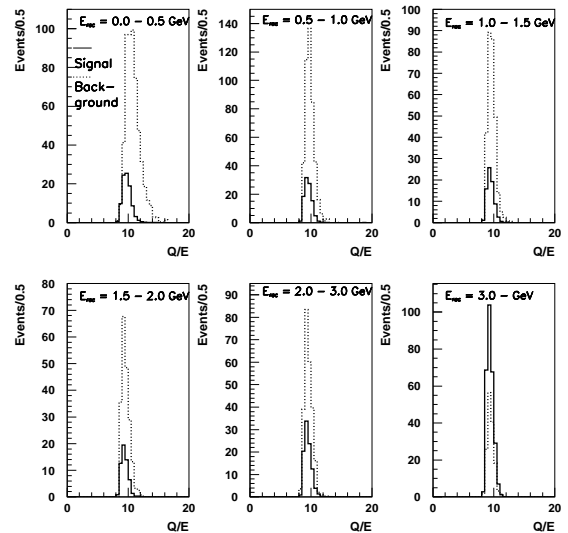


FIG. 7: The distributions of the ratio, the total charge in PE to the ring energy in MeV are shown. The distributions in solid line are for the signal and those in dotted line are for the background.

electron at a comparable energy would have. Figure 8 shows this small but noticeable effect.

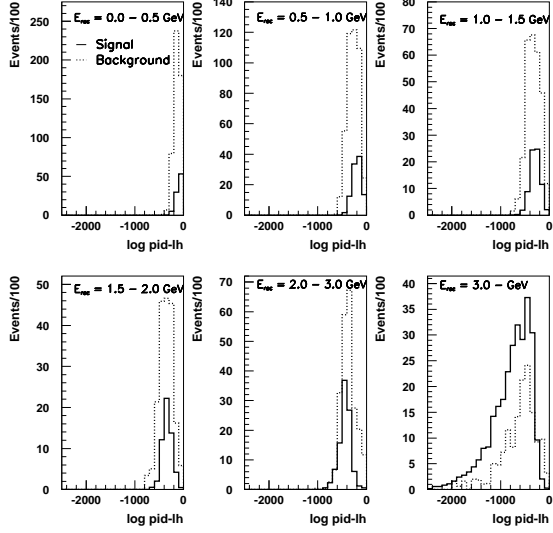


FIG. 8: The distributions of the log-likelihood ratio between e-like and μ -like of the primary e-like ring. The distributions in solid line are for the signal and those in dotted line are for the background.

G. $\log \pi^0$ -likelihood ($\log \pi^0$ -lh)

POLfit provides the logarithm of a likelihood that the event consists of a single π^0 . For events that actually do consist of a single π^0 this variable is expected to be smaller (more negative), namely more π^0 -like, than that for a signal event. This trend shows up in lower energy region ($E_{rec} \leq 1$ GeV) as shown in Figure 9. In the higher energy region, the distribution tends to be narrower for the signal events.

H. Cherenkov angle (Cangle)

The distribution of reconstructed Cherenkov angle is expected to be different between the signal and background events and it depends on whether there is overlap between two Cherenkov rings and on the energy of the primary ring. In Figure 10 the Cherenkov angle distributions for different E_{rec} regions are shown. The shape of the distribution for the signal events differs from that for the background events in most of the energy regions, although degrees of differences vary from energy region to region.

I. Log ring-count likelihood ratio ($\Delta \log$ ring-lh)

To decide how many Cherenkov rings there are in an event, two hypotheses are compared: the first hypothesis is that there is only one Cherenkov ring and the second is

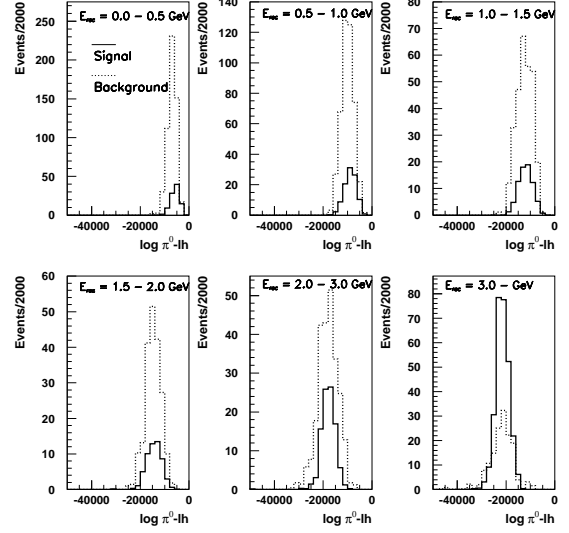


FIG. 9: The distributions of the $\log \pi^0$ -likelihood of single e-like ring events. The distribution in solid line is for the signal and that in dotted line is for the background.

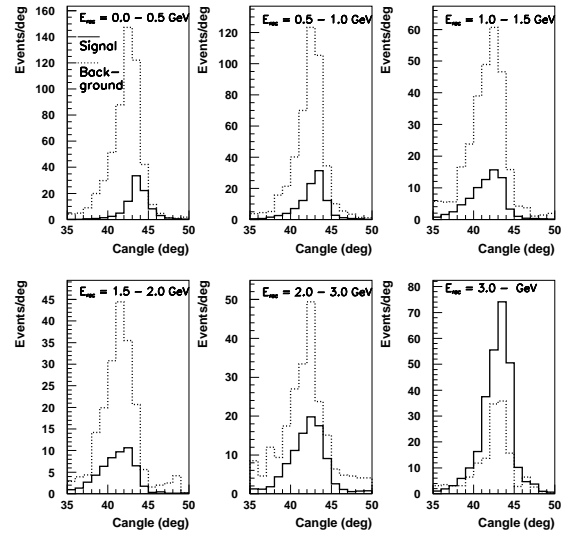


FIG. 10: The distributions of the measured Cherenkov angle of the primary e-like ring. The distribution in solid line is for the signal and that in dotted line is for the background.

that there is an additional ring in the event. The comparison is made using log-likelihood ratio, calculated by the standard SK-I codes, of the two hypotheses. In Figure 11 this log-likelihood ratio is plotted for different E_{rec} regions. The shape of the distribution for the signal events differs from that for the background events in most of the energy regions, although degrees of differences again

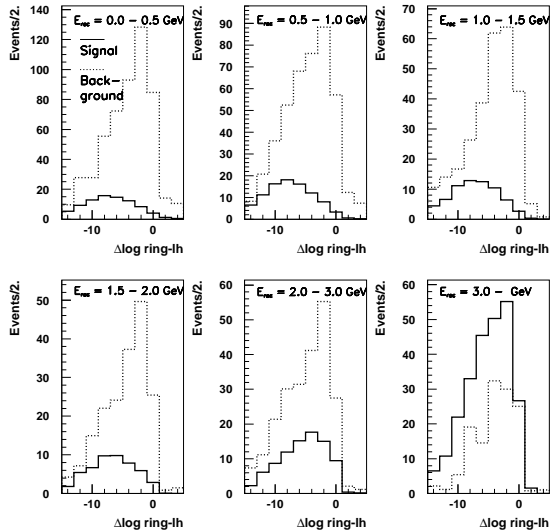


FIG. 11: The distributions of log-likelihood ratio of two hypotheses on the number of Cherenkov ring in an event: there is only one Cherenkov ring or there are more. If the log-likelihood ratio is negative, the event is less likely to have an additional ring. The distributions in solid line are for the signal and that in dotted line are for the background.

vary over the different energy regions.

VII. DISCRIMINATOR: LIKELIHOOD FUNCTION AND LIKELIHOOD RATIO

A series of cuts on the variables described in the previous section can reduce the background well. However, too many cuts in series reduce the signal selection efficiency. The problem for this analysis is that none of the variables alone can separate the signal from the background powerfully. Thus, this situation is well suited for a multivariate analysis where a likelihood function is defined and utilizes all variables that have noticeable distinguishing power. We have shown that the nine variables described above are distributed differently depending on the source of the events (signal or background), although the differences may not be large. As we will see, an accumulation of relatively small differences, when the correlations among the variables are small, can make a bigger difference.

From each distribution shown in Figures 3-11, a probability is calculated for an event to have a value of the corresponding variable i as signal p_i^s and as background p_i^b . Then the log-likelihood is defined by $\log(L_s) = \sum_{i=1,\dots,9} \log(p_i^s)$ as signal and by $\log(L_b) = \sum_{i=1,\dots,9} \log(p_i^b)$ as background. These probabilities are calculated in the same bins of E_{rec} as used in Figures 3-11.

Then the difference between two log-likelihoods,

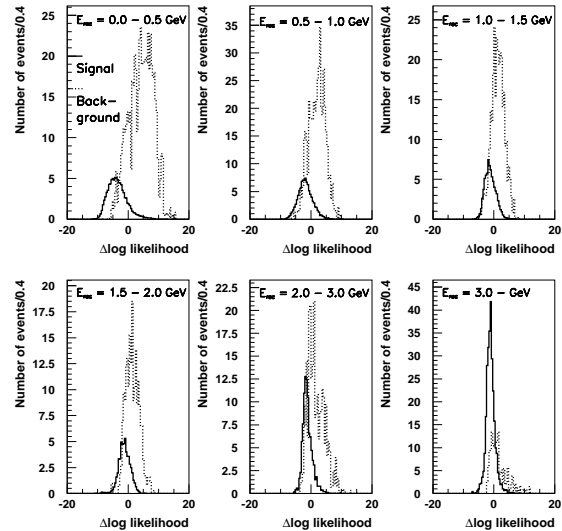


FIG. 12: The distributions of log-likelihood ratio of two hypotheses on the origin of events: signal vs. background. The distributions in solid line are for the signal and those in dotted line are for the background.

$\Delta \log(L) = \log(L_b) - \log(L_s)$, is calculated to decide whether to accept or reject the event. Figure 12 shows $\Delta \log(L)$ distributions for the different E_{rec} regions for the signal events (solid line) and the background events (dotted line). The smaller $\Delta \log(L)$ is, the more likely an event is a signal event. It is clearly seen that the $\Delta \log(L)$ distribution of the signal events differ significantly from that of background events over wide range of E_{rec} .

VIII. RECONSTRUCTED NEUTRINO ENERGY DISTRIBUTIONS WITH A CUT ON $\Delta \log(L)$

The final acceptance of an event is determined by its value of $\Delta \log(L)$. As the distributions of the nine variables used to define the likelihood depend on E_{rec} , so does the distribution of $\Delta \log(L)$. Therefore, in order not to change the energy spectrum unnecessarily, we adopt a strategy to keep the signal detection efficiency constant over a wide range of E_{rec} by changing the $\Delta \log(L)$ cut according to E_{rec} . The cut is selected to retain 40% of the signal that passes the standard SK-I cuts for all E_{rec} .

In presenting the results, first we illustrate the performance of the traditional analysis represented by the standard SK-I codes for comparison. Figure 13 (top) shows the E_{rec} distributions of the signal (dashed line), of the background (background-1) mostly from NC interactions (dotted line), and of the irreducible background (background-2) from the ν_e contamination in the neutrino beam (dash-dotted line). The signal is overwhelmed by the background, especially in the low energy region. In this case, we find 700 signal events, 1,877 background

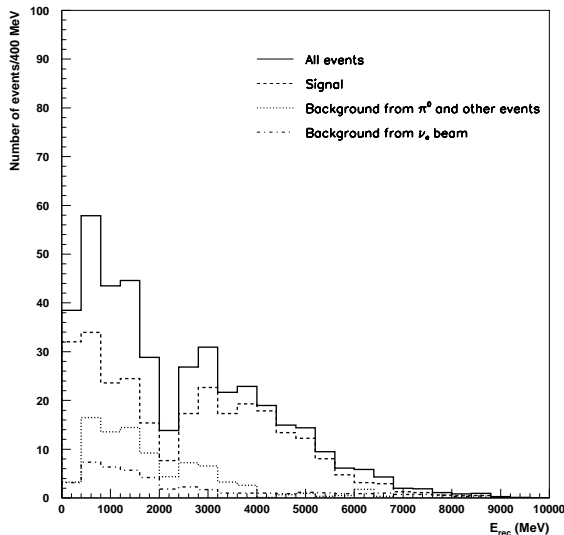
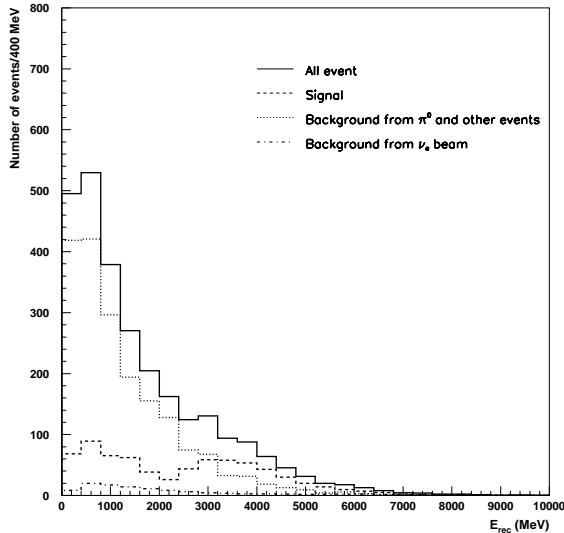


FIG. 13: Top: The distributions of the reconstructed neutrino energy with the standard Super-Kamiokande cuts. The distributions in dashed line are for the signal and those in dotted (dash-dotted) line are for the background-1(-2). $\delta_{CP} = +45^\circ$ and the baseline is 2,540 km. Bottom: The same distributions except that, in addition to the standard Super-Kamiokande cuts, the cut on $\Delta \log L$ is applied.

events from background-1, and 127 background events from background-2.

On the contrary, if we retain 40% of the signal events after the cut on $\Delta \log(L)$ introduced in this paper, the background-1 events are strongly suppressed as shown in Figure 13 (bottom). We find 280 signal, 87 background-1, and 45 background-2 events.

The analysis presented here uses nine variables to define the likelihood. The usefulness of all nine vari-

TABLE I: Summary of the numbers of the signal and background events, and the signal-to-background ratio using events from background-1 with the cut on $\Delta \log(L)$ to retain 40% of the signal events. The signal-to-background ratio with one variable removed is compared to the ratio with all nine variables. Note that the numbers of the signal (background-2) events are not always 280 (45) due to the finite bin size used for the distribution of the variable removed.

Variable removed	Sig	Bkg-1	Bkg-2	Sig/Bkg-1
None	280	87	45	3.22
$\Delta \log \pi^0$ -lh	281	102	45	2.75
Q/E	281	94	45	2.98
$\log \pi^0$ -lh	278	94	47	2.98
$\log \text{pid}$ -lh	277	94	42	2.96
E_{frac}	281	98	45	2.85
$m_{\gamma\gamma}$	280	105	45	2.66
$\cos\theta$	279	101	45	2.76
Cangle	280	98	45	2.86
$\Delta \log \text{ring-lh}$	277	95	45	2.93

TABLE II: Summary of the numbers of the signal and background events for different values of δ_{CP} using events from background-1 (Bkg-1) and background-2 (Bkg-2) with the cut on $\Delta \log(L)$ chosen to retain 40% of the signal events. The errors are statistical due to the limited size of the Monte Carlo event sample.

δ_{CP}	Sig	Bkg-1	Bkg-2
$+135^\circ$	386 ± 6	89 ± 8	45 ± 1
$+45^\circ$	280 ± 5	87 ± 8	44 ± 1
0°	197 ± 4	90 ± 8	44 ± 1
-45°	159 ± 3	87 ± 8	44 ± 1
-135°	263 ± 3	87 ± 8	45 ± 1

ables is evaluated by examining how much the signal-to-background (S/B) ratio changes when each variable is removed in turn from the overall likelihood function. Table I summarizes the numbers of events and the S/B ratio for each case where only the contribution to background-1 is considered. The S/B ratio is always appreciably smaller when one of the nine variables is removed from the likelihood function than when all nine are included. Each variable helps to enhance the signal.

IX. E_{rec} DISTRIBUTIONS AND CP-VIOLATING PHASE δ_{CP}

In the previous section we showed that with a set of appropriate cuts, the background contribution can be suppressed down to a reasonable level, while retaining enough statistics for the signal. In this section, we see whether this set of the cuts is still useful for other values of the CP-violating phase δ_{CP} . Table II lists the numbers of events from the signal, background-1 and background-2 for various values of δ_{CP} .

XI. SOURCES OF BACKGROUND EVENTS

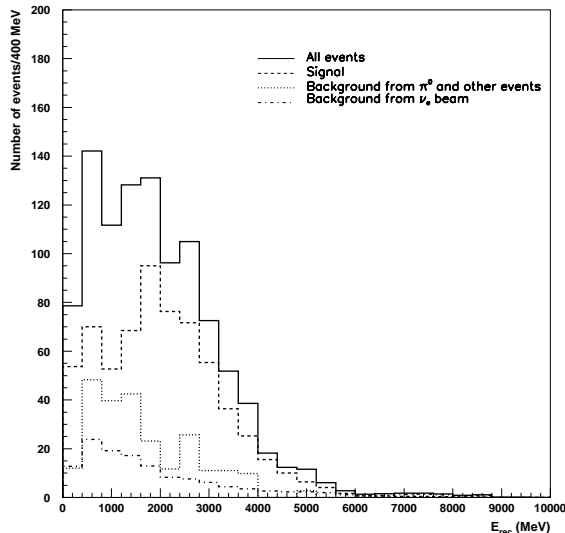


FIG. 14: The distributions of the reconstructed neutrino energy is shown for events that pass the standard SK-I cuts and the cut on $\Delta \log(L)$ such that 40% of the signal events are retained. The distributions in dashed line are for the signal and those in dotted (dash-dotted) line are for the background-1 (background-2). $\delta_{CP} = +45^\circ$ and the baseline is 1,480 km.

TABLE III: Summary of the numbers of signal and background events for different values for δ_{CP} using events from background-1 (Bkg-1) and background-2 (Bkg-2) with the cut on $\Delta \log(L)$ to retain 40% of the signal events and using a baseline of 1,480 km. The errors are statistical due to the limited size of the Monte Carlo event sample.

δ_{CP}	Sig	Bkg-1	Bkg-2
$+135^\circ$	646 ± 9	238 ± 23	133 ± 2
$+45^\circ$	698 ± 11	235 ± 23	133 ± 2
0°	498 ± 8	230 ± 23	132 ± 2
-45°	356 ± 6	250 ± 24	134 ± 2
-135°	609 ± 9	237 ± 23	134 ± 2

X. E_{rec} DISTRIBUTIONS AND BASELINE

It is interesting to see how the baseline will change the results of similar analyses presented in the preceding section. For this study, the cut on $\Delta \log(L)$ is used again to retain 40% of signal and the baseline is assumed to be 1,480 km (Fermilab to Henderson Mine). Figure 14 shows the E_{rec} distribution of the signal (dashed line), background-1 (dotted line) and background-2 (dash-dotted) for $\delta = +45^\circ$. Table III lists the numbers of events from the signal, background-1 and background-2 for different values of δ_{CP} .

It is important to know where the background events come from. Information such as the true energy of neutrinos and nature of interaction of neutrinos that produce the background events is very useful for design of the neutrino beam for a VLBNO experiment.

Figures 15-16 show the neutrino energy distributions of the signal, background-1 and background-2 events for the baseline of 2,540 km and 1,480 km, respectively. These events are chosen with the $\Delta \log(L)$ cut that retains 40% of the signal events after the first set of the cuts (the standard SK-I cuts).

As mentioned earlier, for the most of the results presented in this report, we apply the cut on the neutrino energy at 10 GeV. To justify this cut, we checked to see how much more the background contribution would increase if we allowed events produced by neutrinos whose energies were greater than 10 GeV and less than 15 GeV. For these additional events we fixed the weight value to that used at 10 GeV. The atmospheric ν_e flux times the ν_e cross section decreased by about 60% while that for the wideband ν_μ beam by about 50% in this energy region. Therefore the atmospheric ν_e and ν_μ spectrum are only slightly softer than the wideband ν_μ spectrum from 10 GeV to 15 GeV. This argument, therefore, gives a reasonable estimate of the extra contribution from high energy neutrinos. All the neutrino oscillation parameters are the same as in the case with $\delta_{CP} = +45^\circ$, the baseline of 2,450 km, and the 40% $\Delta \log(L)$ cut. The numbers of the signal, background-1, and background-2 events accepted are 281, 91 and 45, respectively, which should be compared with 280 for the signal, 87 for the background-1 and 45 for the background-2 with the neutrino energy cut at 10 GeV. Thus the percent increases in the number of the signal, background-1 and background-2 events are 1%, 4%, and 0%, respectively.

Tables IV and V summarize all neutrino interactions that produce candidate events passing all cuts with 40% efficiency for the baseline of 2,540 km and 1,480 km, respectively. In these tables, π^0, π^\pm , and $n\pi$ stand for single π^0 , single π^\pm and multiple π production, respectively. The $co\pi$ label stands for π production via coherent interaction with the oxygen nucleus. The “others” includes eta and kaon production as well as deep inelastic scattering (DIS). However, for the background, the label “ $n\pi$ ” includes DIS. Note that in the tables there is no contribution From NC interaction for signal events by definition. CC QE contributions to background-1 are due to ν_μ interactions. Since the cross section of the coherent pion production is known only to an accuracy of $\pm 30\%$ (see reference [3]), we estimate the effect of this error on our background-1 contribution by varying the cross section by $\pm 30\%$. For $\delta_{CP} = +45^\circ$ with the baseline of 2,450 km $\pm 30\%$ changes in this cross section result in changes in the numbers of background-1 events by $\pm 3\%$.

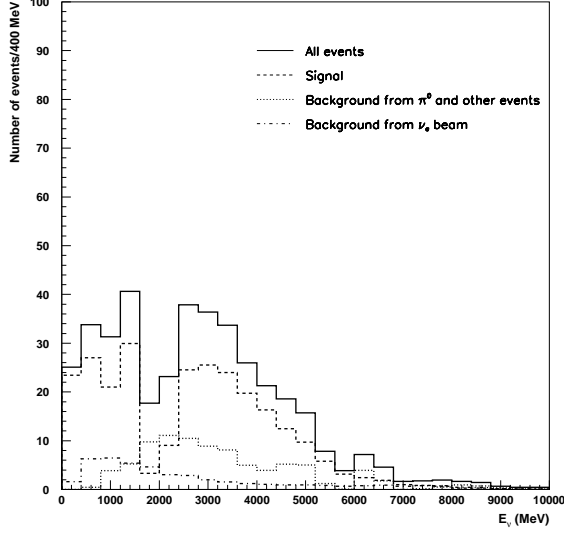


FIG. 15: The distribution of the energies of neutrinos that produce the signal, background-1 and background-2 events. In addition to the standard Super-Kamiokande cuts, the cut on $\Delta \log(L)$ is applied in such a way to retain 40% of the signal events that survive by this cut. The distribution in dashed line is for the signal and that in dotted (dash-dotted) is for the background-1(-2). $\delta_{CP} = +45^\circ$ and the baseline is 2,540 km.

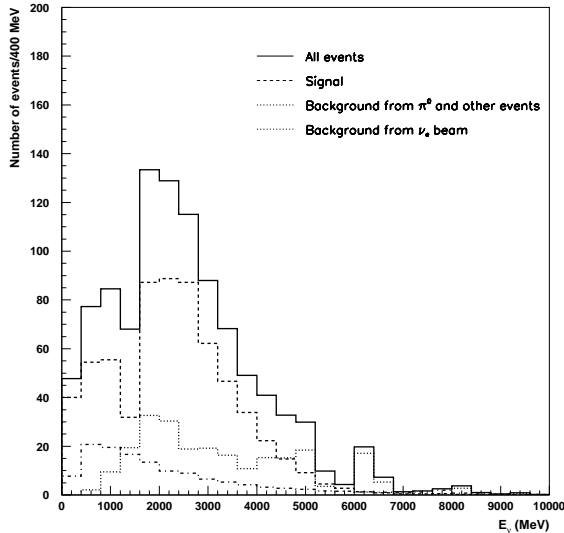


FIG. 16: The distribution of the energies of neutrinos that produced the signal, background-1 and background-2 events. In addition to the standard Super-Kamiokande cuts, the cut on $\Delta \log(L)$ is applied in such a way to retain 40% of the signal events that survive by this cut. The distribution in dashed line is for the signal and that in dotted (dash-dotted) is for the background-1(-2). $\delta_{CP} = +45^\circ$ and the baseline is 1,480 km.

TABLE IV: The percent contributions from events produced by different interactions for signal events and for the background-1 events are summarized for $\delta_{CP} = +45^\circ$ with the cut on $\Delta \log(L)$ to retain 40% of the signal events and with the baseline of 2,540 km.

Interaction	E_{rec} range (GeV)					
	0.0-0.5	0.5-1.0	1.0-1.5	1.5-2.0	2.0-3.0	3.0-
Sig						
CC QE	86%	79%	63%	82%	28%	46%
CC π^0	2%	3%	4%	2%	5%	6%
CC π^\pm	11%	15%	28%	13%	37%	30%
CC $n\pi$	1%	3%	3%	4%	25%	14%
CC others	0%	0%	1%	0%	3%	2%
Bkg-1						
CC QE	7%	5%	6%	0%	0%	0%
CC π^0	0%	1%	4%	6%	4%	0%
CC π^\pm	2%	5%	0%	1%	0%	0%
CC $n\pi$	0%	0%	3%	6%	0%	0%
CC others	0%	0%	0%	0%	21%	3%
NC π^0	23%	53%	60%	59%	18%	0%
NC π^\pm	64%	10%	6%	0%	0%	0%
NC $n\pi$	0%	13%	5%	16%	55%	92%
NC $co\pi^0$	5%	14%	16%	12%	2%	5%
NC elastic	0%	0%	1%	0%	0%	0%

TABLE V: The percent contributions from events produced by different interactions for the signal events and for the background-1 events are summarized for $\delta_{CP} = +45^\circ$ with the cut on $\Delta \log(L)$ to retain 40% of the signal events and with the baseline of 1,480 km.

Interaction	E_{rec} range (GeV)					
	0.0-0.5	0.5-1.0	1.0-1.5	1.5-2.0	2.0-3.0	3.0-
Sig						
CC QE	82%	77%	52%	42%	54%	53%
CC π^0	3%	3%	6%	7%	4%	5%
CC π^\pm	14%	18%	30%	36%	30%	30%
C $n\pi$	1%	2%	12%	13%	11%	10%
CC others	0%	0%	0%	2%	1%	2%
Bkg-1						
CC QE	8%	4%	1%	3%	0%	0%
CC π^0	0%	2%	6%	4%	0%	0%
CC π^\pm	6%	6%	2%	1%	1%	0%
CC $n\pi$	0%	0%	1%	1%	0%	0%
CC others	0%	0%	0%	4%	2%	7%
NC π^0	23%	58%	61%	29%	23%	0%
NC π^\pm	59%	5%	6%	0%	0%	0%
NC $n\pi$	0%	11%	5%	23%	65%	93%
NC $co\pi^0$	4%	14%	17%	35%	9%	0%
NC elastic	0%	0%	1%	0%	0%	0%

XII. DETECTOR SIZE AND GRANULARITY

It is interesting to see what the effect of the detector size has on the performance of *POLfit*. Although the results reported so far are based on the analyses of the Monte Carlo events generated for the Super-Kamiokande detector with 40% PMT coverage, we can make some assessment of the effect of a larger, more granular de-

detector by imposing a cut on the distance to the PMT surface from the π^0 production point in the direction of the π^0 (D_{wall}). For this study we use single π^0 events produced by NC interactions. When the π^0 energy is about 1 GeV, the minimum opening angle of two photons is about 20° and less at higher energies. As D_{wall} gets larger, the number of PMTs that detect Cherenkov photons increases (improved granularity) which can help to resolve light patterns. Two negative impacts compete with this effect. The Cherenkov cone is more spread out so less light is seen by any one PMT. The light must travel further and is thus more subject to absorption and scattering (attenuation) in the water. These both lead to a decrease in the number of detected photons per PMT which may degrade the pattern of light that the Cherenkov cone produces. In the first case, since information is not lost and is just spread out to more PMTs the problem can likely be handled in improvements to reconstruction codes. In the second case, some information about the original Cherenkov light emitting particles is unrecoverable.

Figure 17 shows the π^0 detection efficiency as a function of the opening angle for D_{wall} ranges: 5 m - 10 m, 15 m - 20 m, and 25 m - 30 m and includes *POLfit* information. It is clearly seen that when the opening angle is smaller (less than 60°), the efficiency is improved as the distance to the PMT surface in the π^0 direction increases. Note that above the opening angle of 60° , the π^0 detection efficiency seems more or less independent of D_{wall} . Because of the finite size of the detector and at such large opening angles selecting events based on D_{wall} becomes a less capable means of emulating a larger detector.

Nevertheless, this indicates that the granularity of the detector in terms of the PMT density is an important factor to improve the π^0 detection efficiency. It also appears that the effect of light attenuation is not a major issue at least for Cherenkov light traveling up to 30-40 m in SK-I water which has an attenuation length of 80-100 m (depending on wavelength).

Therefore for the same PMT coverage using the same PMTs, a larger detector than SK-I will perform better, on average, to reconstruct π^0 . Limitations may be expected once the typical path length for Cherenkov light approaches attenuation length.

A similar study can be done by looking at how the S/B ratio varies as a function of D_{wall} for other event types. In this case we look at the S/B ratio for values of D_{wall} for the primary e-like ring. For $D_{wall} > 20$ m the S/B ratio changes from the average of 1.4 to 3.8 for events with $E_{rec} \leq 1.2$ GeV, and for events with $2 \text{ GeV} \leq E_{rec} < 4 \text{ GeV}$ the S/B ratio essentially stays the same.

The large improvement in the S/B ratio for events with $E_{rec} \leq 1.2$ GeV results from an increase in the number of PMTs (pixels) in a Cherenkov ring. This improvement is significant as in the energy region $E_{rec} \leq 1.2$ GeV the contribution from the NC events is reduced to a level as low as that from the irreducible background. This improvement, however, is not realized for events with 2 GeV

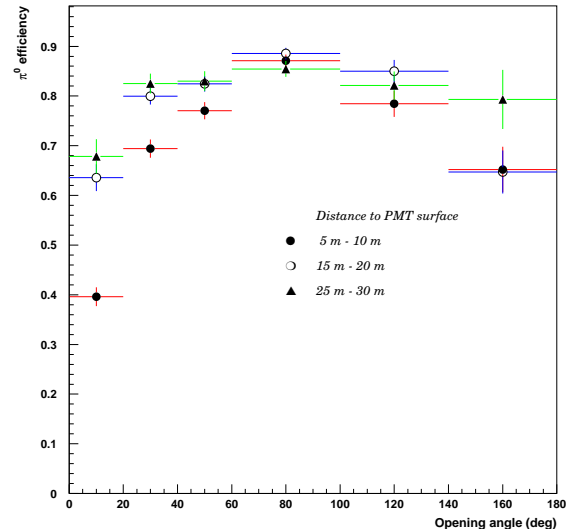


FIG. 17: The π^0 detection efficiency as a function of the two photon opening angle for three ranges of the distance from the π^0 production vertex to the closest PMT surface in the direction of π^0 .

$\leq E_{rec} < 4 \text{ GeV}$ presumably because in this energy region multi-pion events are the major background.

This observation is also true if the minimum distance D_{wall} is set at 10 or 15 m, although the improvement in the S/B ratio is less than the case of the 20-m cut. For a SK-I sized detector, this 20-m cut reduces the number of the signal events by 41%. However, if the detector is larger, this loss of efficiency can be greatly reduced. In other words, for a given detector size, the finer granularity, not necessarily the number of Cherenkov photons collected by individual PMT, improves the S/B ratio.

XIII. CONCLUSION

For the baseline of 2,540 (1,480) km the detection efficiency of the signal events using the SK-I cuts only is found to be 0.361 ± 0.003 (0.373 ± 0.003) and the final efficiency with the further 40% cut on the log-likelihood ratio is found to be 0.145 ± 0.002 (0.149 ± 0.002). The detection efficiency of the background-1 events using the SK-I cuts only is found to be 0.054 ± 0.001 (0.059 ± 0.001) and the final efficiency with the further 40% cut on the log-likelihood ratio is found to be 0.0025 ± 0.0002 (0.0026 ± 0.0003). The 40% cut on the log-likelihood ratio should be considered as a guidance and the actual cut should be optimized after a detailed study of figure of merit that depends on the experimental design including the neutrino beam properties of a given experiment.

We have demonstrated that a large water Cherenkov detector can be used to detect efficiently the signal events by ν_e s from the neutrino oscillation $\nu_\mu \rightarrow \nu_e$ while keep-

ing the background at a reasonably low level in a VLBNO experiment for the baseline of over 1,400 km with a wide-band beam.

Acknowledgments

The authors gratefully acknowledge the work of the Super-Kamiokande collaboration in developing the most of tools used for this analysis. However, the result and

its interpretation are responsibility of the authors of this paper. The work is partially supported by funding from Stony Brook University Office of the Vice President for Research, DOE grant DEFG0292ER40697 at Stony Brook University and DOE contract DE-AC02-98CH10886 at Brookhaven National Laboratory, and the City University of New York PSC-CUNY Research Award Program at Borough of Manhattan Community College/the City University of New York.

-
- [1] D. Beavis *et al.*, Report of the BNL neutrino working group, BNL-69395, hep-ph/0211001; M. V. Diwan *et al.*, Phys. Rev. D68 (2003) 012002, also hep-ex/0303081.
- [2] M. Shiozawa, Nucl. Instr. Meth. A433 (1999) 240.
- [3] Y. Ashie *et al.*, Phys. Rev. D71 (2005) 112005.
- [4] C. K. Jung, Feasibility of a Next Generation Underground Water Cherenkov Detector: UNO, Talk at NNN99, Stony Brook, New York, 1999, available at arXiv:hep-ex/0005046. Also see the expression of interest and the proposal by the UNO collaboration available at <http://nngroup.physics.sunysb.edu/uno/publications.shtml>
- [5] B. Viren. <http://www.phy.bnl.gov/trac/nuosc/>.
- [6] Dziewonski and Anderson, Preliminary Reference Earth Model, Phys. Earth. Planet. Int., 25, 297-356 (1981).
- [7] I. Mocioiu, R. Shrock, Matter Effects on Neutrino Oscillations in Long Baseline Experiments, Phys.Rev. D62 (2000) 053017 and I. Mocioiu, R. Shrock, Neutrino Oscillations with Two Δm^2 Scales, JHEP 0111, (2001) 050.
- [8] T. Barszczek, Ph.D Thesis, University of California, Irvine, unpublished (2005). Available at the Super-Kamiokande website at <http://www-sk.icrr.u-tokyo.ac.jp/sk/pub/index.html>.
- [9] Y. Itow *et al.*, The JHF-Kamioka neutrino project, KEK report 2001-4, ICRR-report-477-2001-7, TRI-PP-01-05, hep-ex/0106019 (2001); C. Yanagisawa, Background Understanding and Suppression in Very Long Baseline Neutrino Oscillation Experiments with Water Cherenkov Detectors Talk at NNN05, Aussois, France, 2005, available at <http://nnn05.in2p3.fr/schedule.html/>.